

RESEARCH

Open Access



Potassium citrate-derived porous carbon with high CO₂ capture and Congo red adsorption performance

Song Wang¹, Tingting Zhang^{1†}, Jiaxin Li^{2†}, Yumeng Hua¹, Jiali Dou¹, Xuecheng Chen^{2*} and Sanxi Li¹

Abstract

The objective is to achieve the goal of carbon neutrality, controlling CO₂ emissions is a primary problem to be solved in the current environmental protection field. Eliminating the environmental pollution of dyes in industrial wastewater is also an urgent problem to be solved in the field of environmental protection. The adsorption technique is an effective way to deal with these two issues. Developing high-efficiency adsorbents is an essential work in the adsorption field. In this work, a simple carbonization method has been developed to prepare porous carbon. The morphology and structure of the prepared porous carbon were investigated by scanning electron microscopy, X-ray photoelectron spectroscopy, X-ray diffraction, and surface area measurement. By studying the influence of preparation conditions on the structure and properties of the prepared carbon materials, it was found that the carbon materials prepared at 900 °C (PCMCA-900) exhibited a high specific surface area of 1476 m² g⁻¹ and a high total pore volume of 0.951 cm³ g⁻¹. The PCMCA-900 showed the highest CO₂ uptake of 7.67 mmol g⁻¹ at 0 °C and the adsorption capacity of PCMCA-900 decreased by less than 5% after 10 times recycling. Moreover, when PCMCA-900 was used as an adsorbent to remove Congo red in water, an adsorption capacity of 652.3 mg g⁻¹ was achieved. Therefore, potassium citrate-derived porous carbon is a desirable candidate for excellent CO₂ adsorption and Congo red in industrial wastewater.

Keywords Porous carbon, CO₂ capture, Congo red adsorption, Adsorbent, Potassium citrate

Introduction

Various environmental problems have attracted more and more attention this century [1–3]. The greenhouse effect is a significant ecological problem mainly caused by the excessive emission of CO₂ due to the burning of fossil fuels [4–6]. The intensification of the greenhouse effect

can result in the rise in sea level, sharp weather changes, and frequent natural disasters [7]. Therefore, the development of CO₂ utilization and storage technology has become a hot research topic in recent years [8]. Several technologies were developed for CO₂ capture, including chemical absorption with amine or amino-based adsorbent and membrane separation [9–11]. However, these technologies showed some disadvantages, such as the corrosion of equipment and high cost.

Water pollution, especially the organic dye polluted water, is another environmental problem that needs to be solved urgently. Organic dyes are extensively used in textile, printing, and papermaking industries [12, 13]. The accidental discharge of toxic dye wastewater is harmful to human health [14, 15]. Recently, membrane separation, solvent extraction, and chemical precipitation techniques

[†]Tingting Zhang and Jiaxin Li have contributed equally to this work

*Correspondence:

Xuecheng Chen
Xuecheng.Chen@zut.edu.pl

¹ Key Laboratory of Polymer and Catalyst Synthesis Technology of Liaoning Province, School of Environmental and Chemical Engineering, Shenyang University of Technology, Shenyang 110870, China

² Faculty of Chemical Technology and Engineering, West Pomeranian University of Technology, Piastów Ave. 42, 71-065 Szczecin, Poland

have been developed for wastewater treatment [16–19]. The main problems of these technologies are high operation costs and low treatment efficiency. Thus, seeking technology with high efficiency and low cost is highly necessary to solve the state-of-the-art environmental issues.

The adsorption method is regarded as one of the most efficient methods that can be used not only to capture CO₂ but also to remove dyes in polluted water. Compared with other methods, the adsorption method has the advantages of low energy consumption, environmental friendly, and simple operation process [20]. Various adsorbents have been developed, including metal–organic frameworks, covalent organic frameworks, zeolites, porous carbon, etc. [21]. Among these adsorbents, porous carbon adsorbent is favored by researchers because of their large specific surface area, adjustable pore structure, lower preparation cost, and abundant source [22, 23]. The abundant pore structure makes these adsorbents promising materials in CO₂ capture or dye adsorption [24–26]. Meanwhile, these reusable carbon materials can be used not only as the adsorbent for CO₂ and dyes, but also as catalysts, supercapacitor, etc. [27–29]. Thus, developing high-performance carbon materials has become a research focus.

Recently, more and more attention has been paid to the high value-added products prepared from biomass-derived material [30–32]. Porous carbon adsorbent can be obtained from biomass-derived materials, such as coconut shell [33], lotus stem, maple leaf, garlic peel, and nutshell [34, 35]. Using these biomass-derived materials to prepare porous carbon adsorbents can not only reduce the production cost but also promote the comprehensive utilization of biomass resources. Citric acid is a valuable chemical product with high content of carbon elements, which can be extracted from biomass resources, such as the peel of grapefruit, orange, etc. With the maturity of industrial fermentation technology for citric acid production, there are more and more studies on the application of citric acid [36]. Moreover, potassium citrate can be used as an activator to prepare porous carbon. It was reported, when poplar catkin was activated by potassium citrate, the surface area of the prepared carbon material reached 2186 m² g⁻¹ [37]. So far, there are no studies on using potassium citrate-derived porous carbon adsorbent to capture CO₂ and adsorb dyes simultaneously.

Here, we reported an effective strategy to prepare a porous carbon from potassium citrate with a high specific surface area (1476 m² g⁻¹) and pore volume (0.951 cm³ g⁻¹), as well as abundant oxygen functional group on its surface. The effect of carbonization temperature on the adsorbent structure was investigated. When used as the adsorbent for CO₂, PCMCA-900, which was

prepared at 900 °C, exhibited the highest CO₂ adsorption capacity of 7.67 mmol g⁻¹ at 0 °C and stable recycling stability. In addition, the PCMCA-900 showed the high Congo red adsorption of 652.3 mg g⁻¹ in water.

Experimental section

Materials

Analytical grade potassium citrate monohydrate (PCM) was bought from Tianjin Damao chemical reagent company and used directly without purification.

Preparation of porous carbon adsorbent

First, 3 g PCM was heated at 300 °C for 30 min in a tubular furnace under the N₂ atmosphere. Then, the temperature of the tubular furnace was raised to carbonization temperature ranging from 700 to 900 °C and kept at the carbonization temperature for 30 min. The yield of the obtained residual was about 68%. Finally, the black solid residual was repeatedly washed with distilled water to neutral. The obtained PCM-derived carbon adsorbent was dried at 120 °C for 1 h and named PCMCA-X, where PCMCA indicated the PCM-derived carbon adsorbent and X presented the carbonization temperature. For instance, when the carbonization temperature was 900 °C, the obtained adsorbent was named PCMCA-900. The preparation procedure is shown in Fig. 1a.

Characterization

A scanning electron microscope (SEM, Phenom ProX) was used to observe the surface morphology of the prepared adsorbent. The graphitization degree and crystal structure of the samples were analyzed by Raman spectrometer (RS, T6400) and X-ray diffractometer (XRD, D8). The elemental composition on the surface of the adsorbent was characterized by an X-ray photoelectron spectroscope (XPS, ESCALAB 250) using Al K α radiation. A Quantachrome Autosorb-1C-BP analyzer was used for nitrogen adsorption/desorption. The specific surface area was calculated by the BET method, and the pore size distribution curve was calculated by density functional theory (DFT).

CO₂ adsorption measurement

A static CO₂ adsorption experiment of adsorbent was carried out on the Quantachrome Autosorb-1C-BP analyzer from 0.01 to 1 bar for 5 h at 0 °C, 25 °C, and 50 °C, respectively. Before the CO₂ adsorption experiment, the adsorbent was degassed at 250 °C under a vacuum of 1 × 10⁻⁶ mbar for 1 h. The reusability of the adsorbent was examined with the same instrument at 0 °C for 10 cycles.

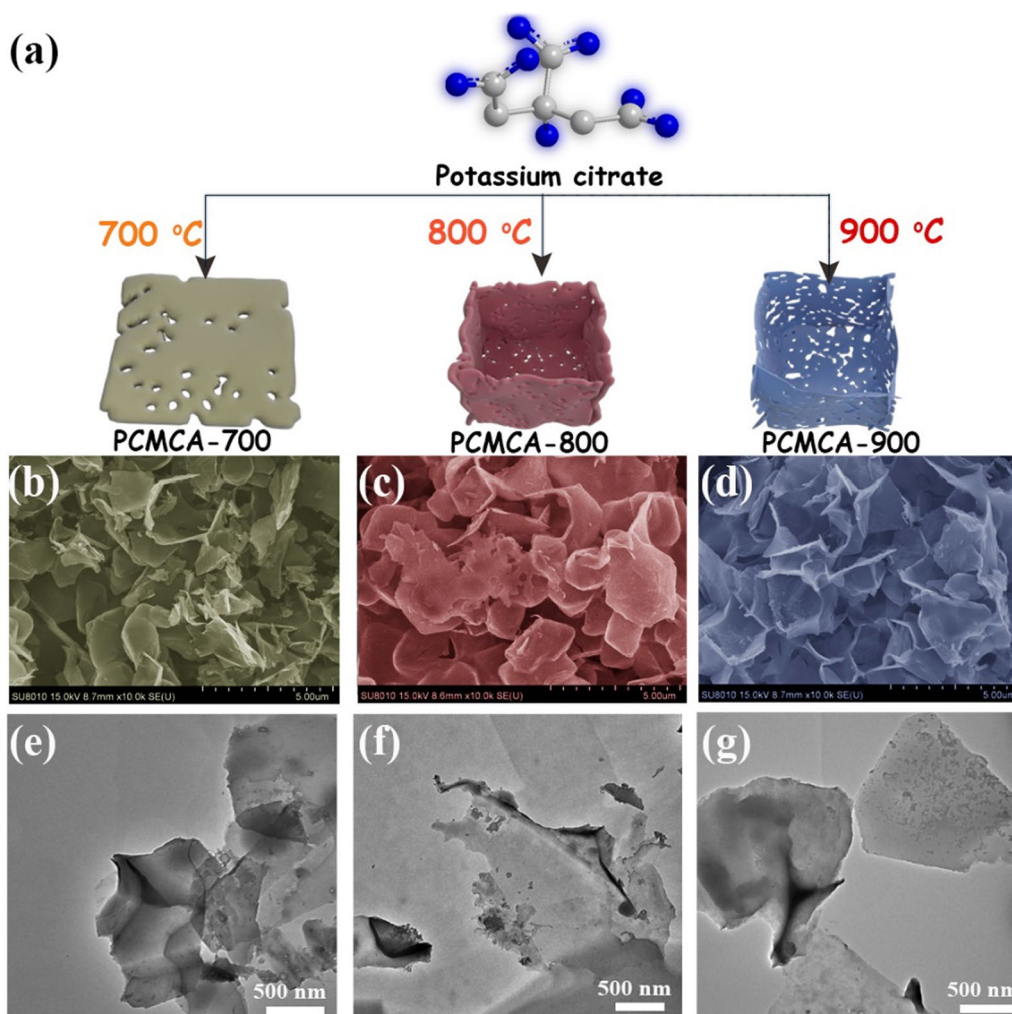


Fig. 1 a Preparation process of PCM-derived hierarchical porous carbon adsorbent; **b–d** SEM images and **e–g** TEM images of PCMCA-X

Congo red adsorption measurement

The CR adsorption performance of the adsorbent was conducted in a batch adsorption process. During the isotherm experiments, 10 mg adsorbent was added into 100 mL CR solution with different concentrations (50, 100, 150, 200, 200 and 300 mg L⁻¹). Then, the mixture was shaken in a thermostatic shaker at 35 °C, which is a temperature close to the actual application environment that is often used in adsorption research [38, 39]. After equilibrium adsorption for 25 h, the suspension was filtered with a 0.22 μm syringe filter. The adsorption capacity (Q_e) of the adsorbent was calculated using the following equation:

$$Q_e = \frac{(C_0 - C_e) \times V}{m} \quad (1)$$

where C_0 (mg L⁻¹) is the initial CR concentration, C_e (mg L⁻¹) is the equilibrium CR concentration, V (mL) is the solution volume, and m (mg) is the adsorbent weight. In the kinetic experiments, the effect of the adsorption time (from 0 to 25 h) on the CR adsorption was examined with the initial concentration of 50, 100, and 200 mg L⁻¹. An ultraviolet spectrophotometer (JC-UT 2000) was used to determine the CR concentration at the wavelength of 497 nm. The recyclability experiment of PCMCA-900 was carried out according to the procedure reported in literatures [40].

Results and discussion

Morphology and nanostructure of PCMCA-X.

To illustrate the influence of the carbonization temperature on the structure of the PCM-derived carbon materials, an SEM examination of the morphology was carried

out first, and the results are shown in Fig. 1b–d. The obtained PCM-derived carbon materials showed similar morphology. These carbon materials were the aggregate of some nanosheets and irregular hollow boxes. The formation of these structures is related to the template effect from K_2CO_3 [27]. With the thermal decomposition of PCM, K_2CO_3 and carbon can be produced, and the K_2CO_3 particles are usually coated by carbon. After the removal of K_2CO_3 during the following water washing procedure, the irregular hollow box-like carbon can be obtained. In PCMCA-700 and PCMCA-800, since the carbonization temperature is relatively low, some irregular hollow box-like carbon can be found. While in PCMCA-900, due to the thermal decomposition of the irregular hollow box-like carbon at high temperature, the aggregate of nanosheets can mainly be observed. These irregular nanosheets can also be found from the TEM images (Fig. 1e–g), and with the increase of carbonization

temperature, it is more conducive to the formation of micropores.

Characterization of PCMCA-X.

Figure 2a shows the Raman spectrum of the prepared samples, from which the D peak at 1340 cm^{-1} and the G peak at 1592 cm^{-1} can be seen [41]. The ratio of I_D/I_G reflects the defect degree of the carbon material. The higher the ratio, the more defect structures in the carbon material. The largest I_D/I_G of PCMCA-900 indicates that it has more defect structures. These defects are caused by a large number of micropores generated by the increase in carbonization temperature. The XRD patterns of the prepared samples are recorded in Fig. 2b. There are two broad diffraction peaks at 2θ of 26° and 43° , which correspond to the (002) and (101) crystal planes of amorphous carbon, respectively [42].

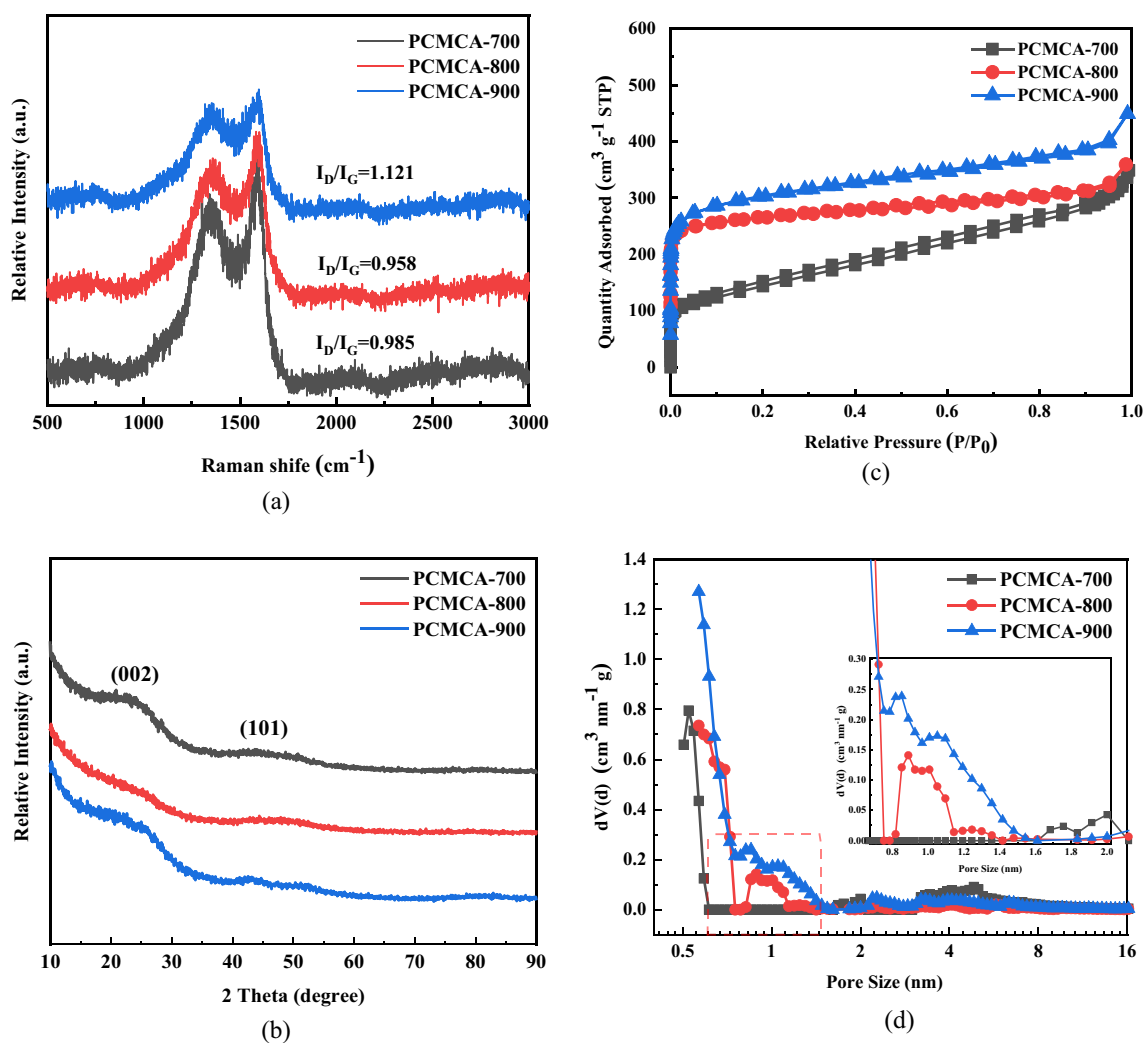


Fig. 2 a Raman curves; b XRD profiles; c N_2 adsorption/desorption isotherms and d pore size distribution curves of the prepared samples

The textural properties of PCM-derived carbon materials were determined by the N_2 adsorption/desorption method. As shown in Fig. 2c, PCMCA-700 shows a type-IV isotherm with an H4 type hysteresis loop, which means that PCMCA-700 is a mesoporous carbon material [43]. The isotherms of PCMCA-800 and PCMCA-900 exhibited a typical type I isotherm. Compared with PCMCA-800, the isotherm curve of PCMCA-900 presents relatively high nitrogen adsorption in the low pressure range ($P/P_0 < 0.05$), which indicates the formation of a more microporous structure in PCMCA-900 [44]. Meanwhile, a wide adsorption knee can be observed in the isotherm curve of PCMCA-900, demonstrating that the mesopores are existing in PCMCA-900 [45–47]. Pore size distribution diagrams of PCM-derived carbon materials indicate that most of the pores of PCMCA-700 are distributed in the pore diameter range from 2 to 10 nm, while PCMCA-800 and PCMCA-900 possess somewhat broader pore size distribution with the most of their pores distributed in the pore diameter range from 0.5 to 10 nm (Fig. 2d). Meanwhile, the percentage of the pore diameter around 0.6 nm in PCMCA-800 is a little higher than that of PCMCA-900, which may affect the CO_2 adsorption capacity of PCMCA-800 at low pressure.

To illustrate the difference in textural properties of the three PCM-derived carbon materials, detailed textural parameters of the three adsorbents are listed in Table 1. The BET surface areas of PCMCA-700, PCMCA-800, and PCMCA-900 are calculated to be 506, 1032, and 1476 $m^2 g^{-1}$, respectively. PCMCA-900 shows the highest micropore volume (V_{micro}) of 0.497 $cm^3 g^{-1}$ and total pore volume (V_{total}) of 0.951 $cm^3 g^{-1}$ among the three adsorbents. During the investigation of CO_2 adsorption, it has been reported that the volume of narrow micropores (the pores distributed between 0.7 and 0.9 nm, $P_{0.7-0.9}$) can significantly affect the adsorption result. Usually, the relatively strong interaction between CO_2 and the surface of narrow micropores can greatly improve the CO_2 adsorption capacity [48, 49]. It can be observed from Table 1 that the $P_{0.7-0.9}$ in PCMCA-900 is 19.21%, which is the highest among the three adsorbents. Thus, the high surface areas and suitable pore volume distribution of PCMCA-900 can provide more active surface sites and

diffusion channels for adsorption, which can enhance the CO_2 and CR adsorption performance of PCMCA-900.

The surface element state of the PCM-derived carbon materials were identified by XPS. As shown in Fig. 3a, two peaks appearing at 285 eV and 533 eV, which suggests the main elements in PCM-derived carbon materials are C and O [50]. In Fig. 3b, the high resolution spectra of C 1s can be further fitted into four separate peaks at 284.3 eV, 285.3 eV, 286.5 eV, and 288.6 eV, which was attributed to C–C (C1), C–OH (C2), C=O (C3), and COOH (C4), respectively [51, 52]. The percentage of each component is listed in Table 2. The percentage of the O-containing functional groups (C2, C3, and C4) of the PCMCA-900 sample is highest among the three examined samples, indicating that more O-containing functional groups were introduced in PCMCA-900. With the introduction of O-containing functional groups, the surface properties of carbon materials can be greatly changed, which is beneficial to improve the adsorption performance of carbon materials [53]. In Fig. 3c, The high-resolution spectra of O 1s can be divided into four separate peaks at 531.5 eV, 533.5 eV, 533.6 eV, and 535.0 eV, which can be assigned to carbonyl, ketone or lactone groups (O1), ether or alcohol groups (O2), carboxyl group (O3) and oxygen in water (O4), respectively [54, 55]. The detailed percentage of these components is presented in Table 3. The total percentage of O1 and O2 in the PCMCA-900 sample is the highest among the three samples. Since O1 and O2 are responsible for alkalinity, and O3 is responsible for acidity, the high percentage of O1 and O2 in the PCMCA-900 sample indicates that PCMCA-900 shows more alkalinity properties than the other two carbon materials [25]. The presence of these O-containing functional groups can improve the adsorption properties of PCM-derived carbon materials [51].

CO₂ adsorption analysis

To compare the CO_2 adsorption performance of the PCM-derived carbon adsorbents, the CO_2 isotherms of PCMCA-X were examined at 0 °C, and the corresponding results are presented in Fig. 4a. The static CO_2 adsorption capacities of the three adsorbents at 0 °C and 1 bar are 4.12 $mmol g^{-1}$, 6.52 $mmol g^{-1}$, and 7.67 $mmol g^{-1}$, respectively. The difference in the static CO_2 adsorption

Table 1 Detailed textural parameters of PCM-derived carbon materials

Sample	S_{BET} ($m^2 g^{-1}$)	S_{micro} ($m^2 g^{-1}$)	V_{total} ($cm^3 g^{-1}$)	V_{micro} ($cm^3 g^{-1}$)	$P_{0.7-0.9}$ ^a (%)
PCMCA-700	506	93	0.539	0.044	0
PCMCA-800	1032	909	0.556	0.358	14.47
PCMCA-900	1476	1140	0.951	0.497	19.21

^a Percentage of the pores distributed between 0.7 and 0.9 nm

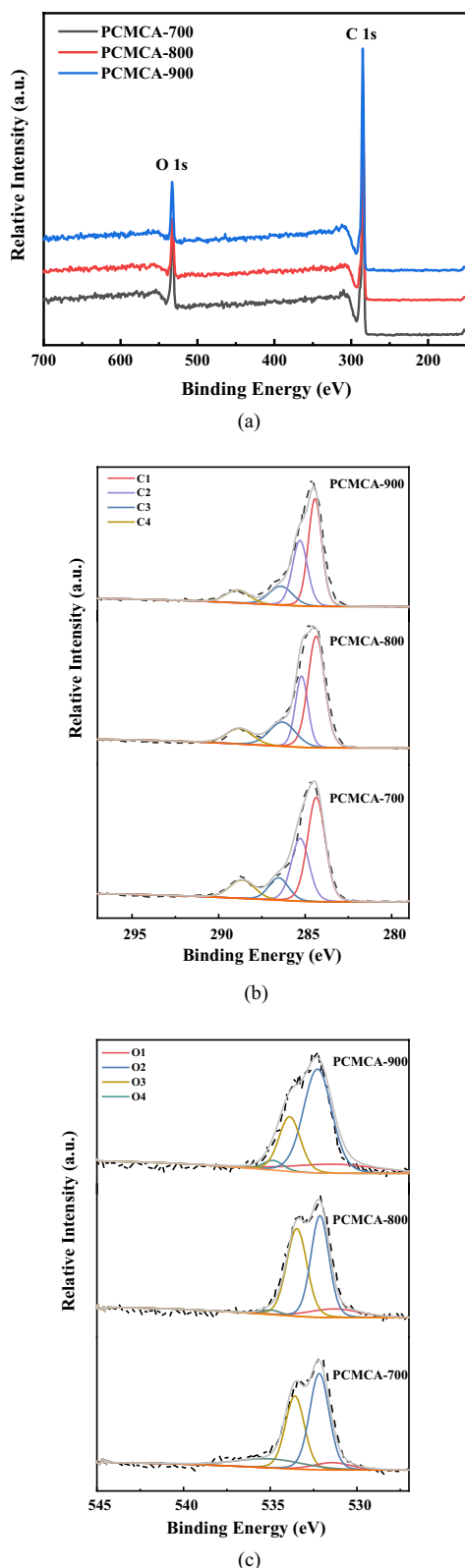


Fig. 3 a XPS full spectra and high-resolution spectra of b C 1 s and c O 1 s of the prepared samples

Table 2 XPS data of C 1 s composition of PCM-derived carbon adsorbents

Sample	C1 (%)	C2 (%)	C3 (%)	C4 (%)
PCMCA-700	47.69	28.98	11.47	11.86
PCMCA-800	48.81	23.55	16.88	10.76
PCMCA-900	45.59	31.06	13.85	9.5

Table 3 XPS data of O 1 s composition of PCM-derived carbon adsorbents

Sample	O1 (%)	O2 (%)	O3 (%)	O4 (%)
PCMCA-700	6.60	45.12	33.57	14.71
PCMCA-800	10.73	44.36	42.82	2.09
PCMCA-900	15.28	57.81	23.14	3.77

capacity of the three adsorbents can be related to their different textural properties. PCMCA-900 has the highest surface area and suitable pore volume distribution, which can not only provide more CO₂ adsorption sites but also provide more CO₂ diffusion channels, leading to the best CO₂ adsorption performance of PCMCA-900 among the three adsorbents. Moreover, as shown in Fig. 4b, S_{BET} of the PCMCA-X materials has a strong influence on the CO₂ capture with a high R^2 of 0.954, indicating the higher specific surface is favor for improvement of CO₂ capture at 0 °C [52].

To illustrate the binding affinity between the PCMCA-900 adsorbent and CO₂, the isosteric adsorption heat was calculated according to the method provided in the literature [52]. The isosteric adsorption heat value of the prepared PCMCA-900 adsorbent is in the range of 22.37 to 27.47 kJ mol⁻¹ in Fig. 4c, which indicates the adsorption of CO₂ on PCMCA-900 adsorbent is a typical physical adsorption process [56]. Thus, the physisorption with relatively low isosteric adsorption heat between CO₂ molecule and the surface of the porous carbon, as illustrated in Fig. 4d, led to the good adsorption performance of PCMCA-900 [57].

Temperature is an important factor affecting the CO₂ adsorption performance of adsorbents. Thus, the influence of adsorption temperature on the CO₂ adsorption performance of PCMCA-900 was explored as well. It can be observed from Fig. 4e that the CO₂ adsorption capacity of PCMCA-900 decreased from 7.67 to 2.11 mmol g⁻¹ when the adsorption temperature increased from 0 to 50 °C [58]. The adsorption capacity of CO₂ decreases with the increase of adsorption temperature. This phenomenon is due to the fact that, when the temperature increases, the surface adsorption energy and molecular

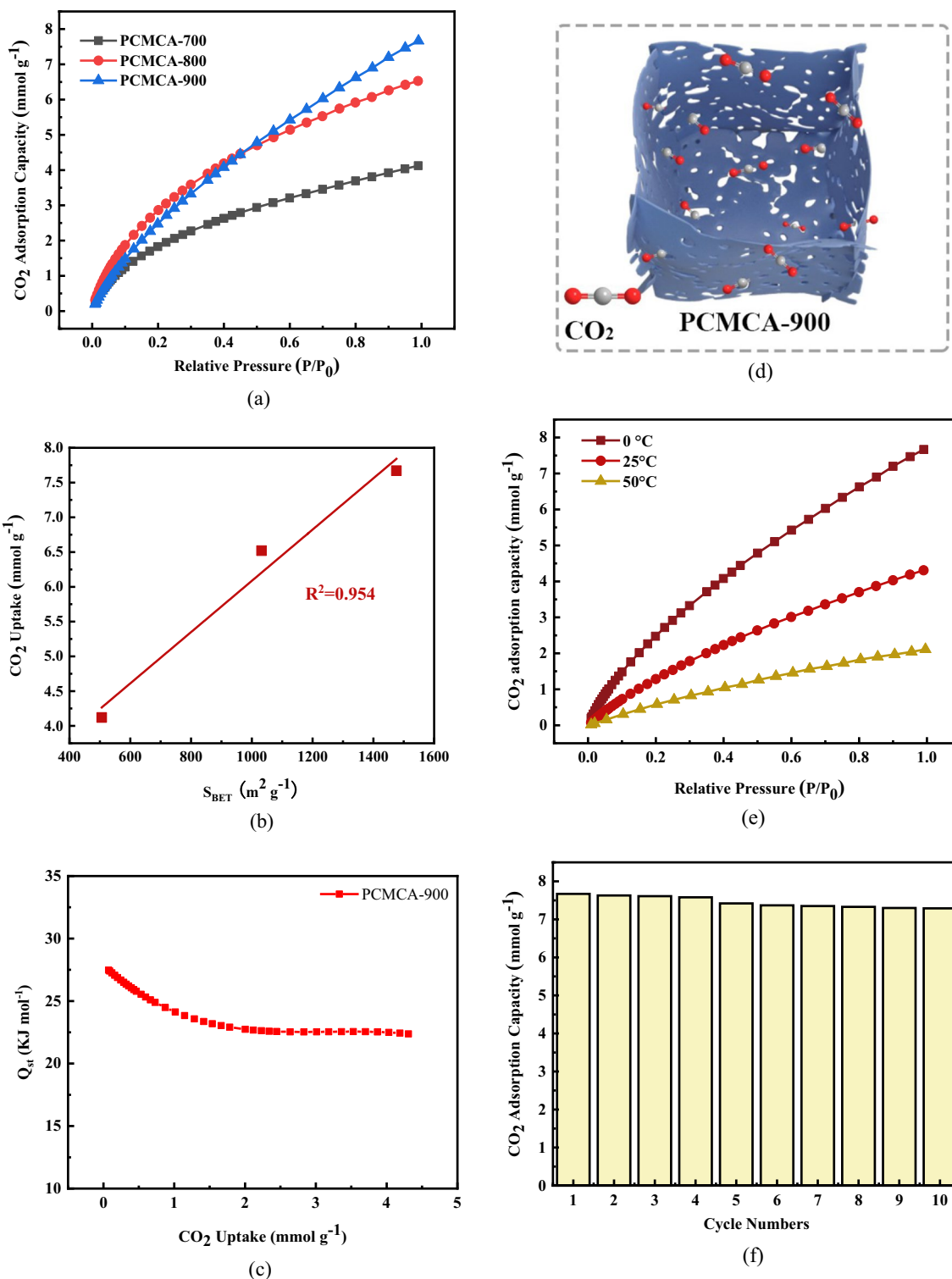


Fig. 4 a CO_2 adsorption isotherms and b S_{BET} vs CO_2 uptake with a fitting line of PCMCA-X samples at 0 °C. c Q_{st} of PCMCA-900. d CO_2 capture mechanism of PCMCA-900. e CO_2 uptake capacities at various temperatures (0 °C, 25 °C, and 50 °C) at 1 bar and f recyclability of PCMCA-900

diffusion rate of CO₂ increase, resulting in the instability between CO₂ and adsorbent and the decrease of CO₂ adsorption capacity [25, 59].

To investigate the recyclability of PCMCA-900, the successive adsorption–desorption experiment was applied. At each cycle, PCMCA-900 was degassed at 250 °C for 1 h under vacuum. Then, PCMCA-900 was cooled to 0 °C to start the next cycle. 10 cycles were carried out to evaluate the recyclability of PCMCA-900. It can be seen from Fig. 4f that, after 10 cycles of CO₂ adsorption and desorption, the CO₂ adsorption capacity decreased by less than 5% (7.67 mmol g⁻¹ to 7.29 mmol g⁻¹), demonstrating the high recyclability of PCMCA-900.

During these years, materials used for CO₂ adsorption have been continuously developed [52, 56, 57]. Table 4 listed some reported materials that used for CO₂ adsorption. It can be observed that most materials exhibited high CO₂ adsorption ability with the CO₂ adsorption capacity between 5 and 7 mmol g⁻¹ at 0 °C. PCMCA-900 showed relatively better CO₂ adsorption capacity of the 7.7 mmol g⁻¹ at 0 °C. Meanwhile, to prepare PCMCA-900, only potassium citrate was needed. Expensive reagents or activator such as sodium lignosulfonate NaNH₂ are not need. The preparation cost of PCMCA-900 is relatively lower than other listed materials. Thus, PCMCA-900 is a relatively good adsorbent for CO₂ adsorption.

Congo red adsorption analysis

Since PCMCA-900 showed good adsorption performance in the CO₂ adsorption, PCMCA-900 was further used in the study of CR adsorption. The adsorption kinetics of the PCMCA-900 for the removal of CR was examined first, and the results are shown in Fig. 5a. The CR

adsorption ability of the PCMCA-900 is greatly affected by the CR initial concentration. When the CR initial concentration was increased from 50 to 200 mg L⁻¹, the CR adsorption capacity of the PCMCA-900 increased from 297.7 to 408.5 mg g⁻¹. In general, adsorption can be divided into physical adsorption and chemical adsorption. To demonstrate the adsorption mechanism of PCMCA-900, the pseudo-first-order and pseudo-second-order kinetic models were used to illustrate the adsorption mechanism [62, 63]. The pseudo-first-order and pseudo-second-order kinetic models can be described in the following equations:

$$\ln(Q_e - Q_t) = \ln Q_e - K_1 t \quad (2)$$

$$\frac{t}{Q_t} = \frac{1}{K_2 Q_e^2} + \frac{1}{Q_e} t \quad (3)$$

where Q_e (mg g⁻¹), Q_t (mg g⁻¹), K_1 (min⁻¹), and K_2 [g (mg min)⁻¹] are corresponding to the adsorption capacity at adsorption equilibrium, the adsorption capacity at time t (min), the adsorption rate constant of the pseudo-first-order, and the adsorption rate constant of the pseudo-second-order, respectively [64]. The simulated results are shown in Table 5. When the isothermal adsorption kinetic data of CR were simulated by the pseudo-second-order model, the obtained correlation coefficient (R^2) was greater than that of the pseudo-first-order model. Meanwhile, the calculated adsorption capacities at adsorption equilibrium ($Q_{e,cal}$) based on the pseudo-second-order model are much closer to the experimental data than that based on the pseudo-first-order model. These results indicate that the pseudo-second-order model is more suitable for describing the CR adsorption behavior of the PCMCA-900. Therefore, the kinetic study results demonstrate that the overall adsorption kinetics of CR by PCMCA-900 is mainly a chemisorption-controlled process and governed by the diffusion time of adsorbate into the narrow pores [65–67].

To illustrate the equilibrium state of CR molecules in the liquid and solid phase at a constant temperature, Langmuir and Freundlich isotherm models were used, which can be, respectively, represented by the following equations [68]:

$$\frac{1}{Q_e} = \frac{1}{Q_m K_L} \frac{1}{c_e} + \frac{1}{Q_m} \quad (4)$$

$$\log Q_e = \log K_F + \frac{1}{n} \log c_e \quad (5)$$

where Q_e (mg g⁻¹), Q_m (mg g⁻¹), C_e (mg L⁻¹), K_L (L mg⁻¹), K_F ((mg g⁻¹)(L mg⁻¹)^{1/n}), and $1/n$ refer to the adsorption capacity of the adsorbent for the adsorbate at

Table 4 Comparison of the CO₂ adsorption capacity of the prepared adsorbent with the reported materials

Adsorbents	Raw materials	CO ₂ adsorption capacity (mmol g ⁻¹)		Reference
		0 °C	25 °C	
PCMCA-900	potassium citrate monohydrate	7.7	4.3	This work
ACDS-800-4	date, KOH	6.4	4.4	[52]
WSC-500-1	water chestnut shell, NaNH ₂	6.0	4.5	[57]
WFW 20	wood waste + food waste, KOH	-	1.5	[60]
CAC-S	sugarcane bagasse, H ₃ PO ₄ , NaOH	5.5	4.3	[25]
SDC 3	sodium lignosulfonate, urea, NaCl	3.8	2.4	[61]
K3-PDC1	bee-collected pollen grains, KOH	5.6	3.4	[56]

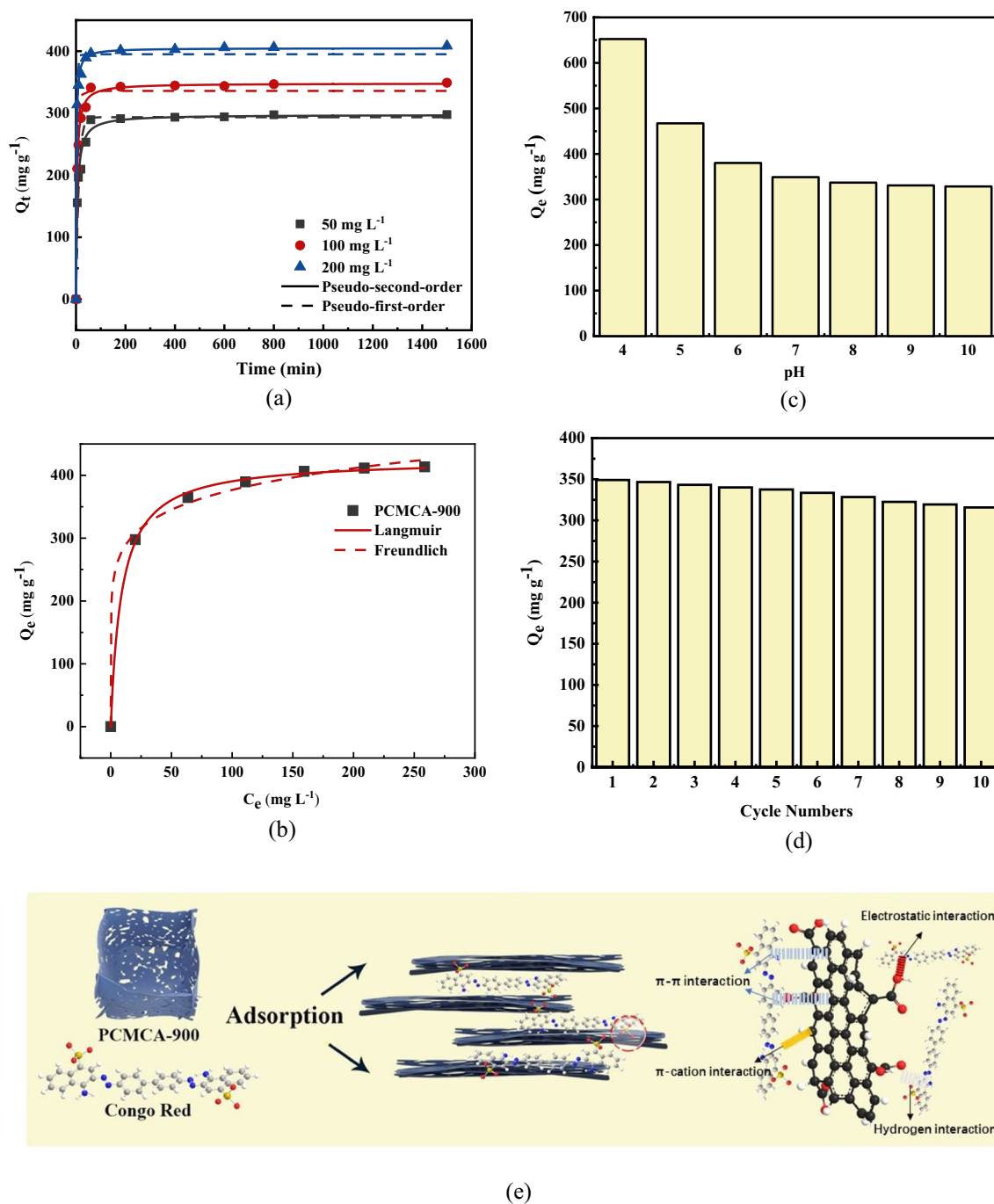


Fig. 5 **a** CR adsorption kinetic by the PCMCA-900 (Conditions: initial concentrations: 50, 100, 200 mg L⁻¹; dosage: 0.1 g L⁻¹; adsorption: 1500 min; temperature: 35 °C). **b** Adsorption isotherms of CR at 35 °C by PCMCA-900 (Conditions: initial concentrations: 50 to 300 mg L⁻¹; dosage: 0.1 g L⁻¹; temperature: 35 °C). **c** Effect of pH values on the CR adsorption capacity of PCMCA-900 (Conditions: initial concentrations: 100 mg L⁻¹; dosage: 0.1 g L⁻¹; temperature: 35 °C). **d** recyclability of PCMCA-900. **e** adsorption scheme for CR of the PCMCA-900

adsorption equilibrium, the maximum adsorption capacity of the adsorbent for the adsorbate, the concentration of adsorbate in solution at adsorption equilibrium, the equilibrium constant in the Langmuir isotherm model, the equilibrium constant in the Freundlich isotherm

model, and the adsorption intensity, respectively [69]. It can be seen from Fig. 5b and Table 6 that the Langmuir model is more suitable for simulating the experimental data due to its high *R*² value of 0.999. Since the Langmuir model is related to the monolayer adsorption, the

Table 5 CR kinetic adsorption fitting parameters

C_0 (mg L ⁻¹)	$Q_{e,exp}$ (mg g ⁻¹)	Pseudo-first-order			Pseudo-second-order		
		$Q_{e,cal}$ (mg g ⁻¹)	K_1 (min ⁻¹)	R^2	$Q_{e,cal}$ (mg g ⁻¹)	K_2 [g (mg min) ⁻¹]	R^2
50	297.7	293.526	0.091	0.905	297.546	0.006	0.987
100	349.1	335.954	0.157	0.972	348.129	0.008	0.996
200	408.2	395.135	0.282	0.983	404.918	0.001	0.998

Table 6 Langmuir and Freundlich isotherm of CR on PCMCA-900

Langmuir model			Freundlich model		
Q_m (mg g ⁻¹)	K_L (L mg ⁻¹)	R^2	K_F [(mg g ⁻¹)(L mg ⁻¹) ^{1/n}]	1/n	R^2
426.037	0.110	0.999	210.649	0.126	0.996

isothermal adsorption results illustrated that CR molecules are adsorbed on the PCMCA-900 surface in the monolayer form at the equilibrium state.

Since the pH value can affect the chemical properties of adsorbent and adsorbate, the effect of pH value on the CR adsorption performance of PCMCA-900 was studied, and the results are presented in Fig. 5c. The CR adsorption capacity of PCMCA-900 is strongly affected by the pH value. With the increase of the pH value of the CR solution, the CR adsorption capacity of PCMCA-900 decreased clearly. The CR adsorption capacity of PCMCA-900 at the pH value of 4 was 652.3 mg g⁻¹, which was about 2 times higher than that at the pH value of 10. This phenomenon can be explained by the different concentrations of H⁺ and OH⁻ ions in CR solution at different pH values. When the pH value of CR solution is lower than 7, with the decrease of solution pH value, the H⁺ ion concentration increases, and the protonation of the PCMCA-900 surface results in the increase of the CR adsorption [65]. When the pH value of the CR solution is higher than 7, the concentration of OH⁻ ion in the CR solution

increases, which can compete with the CR molecule to adsorb on the PCMCA-900, leading to the decrease of the CR adsorption capacity of PCMCA-900 [70].

The recovery of PCMCA-900 is of great importance for its potential application. The recyclability of PCMCA-900 is shown in Fig. 5d. It can be observed that after 10 times recycling, the CR adsorption of PCMCA-900 still reached 315.7 mg g⁻¹, which decreased less than 10% compared with the first-time use. This result indicates that PCMCA-900 is a long-term adsorbent for the removal of CR from the solution.

Figure 5e presents the possible adsorption mechanism of PCMCA-900. The adsorption of CR is mainly due to electrostatic attraction and ion exchange [71]. The benzene ring in CR molecule can interact with porous carbon through π-π stacking, thus facilitating the adsorption of CR. In addition, the -NH₂ group in CR molecule and -OH group in PCMCA-900 can form hydrogen bonds, which is helpful for CR adsorption [72].

Comparison of the CR adsorption capacity of the PCMCA-900 with the reported materials is represented in Table 7. Due to the difference in adsorption conditions, the adsorption ability of different materials can only be roughly compared. It can be observed that the PCMCA-900 and C/MnCuAl-LDOS has relatively good adsorption ability due to their high adsorption capacity of higher than 300 mg g⁻¹. However, the PCMCA-900 showed relative advantages on the aspect of low preparation cost and simple preparation procedure. Thus, the PCMCA-900 is a promising adsorbent for the removal of CR in wastewater.

Table 7 Comparison of the CR adsorption capacity of the prepared adsorbent with the reported materials

Adsorbents	Adsorption conditions	Q_e (mg g ⁻¹)	Reference
PCMCA-900	pH = 7, CR concentration = 100 mg/L,	349.1	This work
C/MnCuAl-LDOS	pH = 4.5, CR concentration = 150 mg/L,	317.2	[65]
GLAC	pH = 3, CR concentration = 50 mg/L,	47.6	[73]
TAC6	pH = 7.2, CR concentration = 100 mg/L,	66.8	[72]
CSP	pH = 7, CR concentration = 100 mg/L	35.0	[26]
NC-5%	pH = 5, CR concentration = 50 mg/L,	99.9	[71]

Conclusions

In summary, a porous carbon adsorbent was prepared from PCM by a simple carbonization method. The obtained PCM-derived carbon adsorbent, PCMCA-900, shows a high specific surface area of $1476 \text{ m}^2 \text{ g}^{-1}$ and a relatively suitable pore size distribution, resulting in excellent performance on CO_2 capture and CR adsorption. The highest CO_2 uptake reached 7.67 mmol g^{-1} , and the highest CR adsorption capacity reached 652.3 mg g^{-1} when PCMCA-900 was used. Therefore, the preparation of PCMCA-900 provided a promising method to utilize biomass-derived material, and developed a high-performance adsorbent, which has the potential application in solving the problems of the greenhouse effect and dye wastewater pollution.

Acknowledgements

The authors are grateful for the financial support from the NCN, Poland, UMO-2020/39/B/ST8/02937.

Author contributions

SW designed the project; TZ and JL completed the experiments, manuscript; YH and JD contributed to the analysis; XC and SL revised the manuscript. All authors read and approved the final manuscript.

Funding

The General Project Fund of Liaoning Education Department (No. LJGD2019014).

Availability of data and materials

Not applicable.

Declarations

Ethics approval and consent to participate

Not applicable.

Consent for publication

Not applicable.

Competing interests

The authors declare that they have no competing interest.

Received: 11 October 2022 Accepted: 7 January 2023

Published online: 08 February 2023

References

- Zhu B, Xu QX, Bao XY, Yin H, Qin YM, Shen XC (2022) Highly selective CO_2 capture and photoreduction over porous carbon nitride foams/LDH monolith. *Chem Eng J* 429:132284
- Lv DW, Yu Q, Xie DN, Zhang JW, Ge XD, Si GY, Zhao B, Wang SX, Larssen T, Duan L (2022) Critical loads of headwater streams in China using SSWC model modified by comprehensive F-factor. *Sci Total Environ* 802:149780
- Guan Y, Xiao Y, Rong B, Zhang NN, Chu CJ (2021) Long-term health impacts attributable to $\text{PM}_{2.5}$ and ozone pollution in China's most polluted region during 2015–2020. *J Clean Prod* 321:128970
- Zhang XW, Zhang X, Liu HL, Li WS, Xiao M, Gao HX, Liang ZW (2017) Reduction of energy requirement of CO_2 desorption from a rich CO_2 -loaded MEA solution by using solid acid catalysts. *Appl Energy* 202:673–684
- Xiao M, Liu HL, Idem R, Tontiwachwuthikul P, Liang ZW (2016) A study of structure-activity relationships of commercial tertiary amines for post-combustion CO_2 capture. *Appl Energy* 184:219–229
- Zhang YQ, Zhang AL, Wang YJ, Wang S, Li SX (2022) Preparation and characterization of LCT/SPEEK composite membrane for PEMFC application. *ChemistrySelect* 7(43):e202202398
- Sun XG, Zhao YL, Qiu JP, Xing J (2022) Review: alkali-activated blast furnace slag for eco-friendly binders. *J Mater Sci* 57(3):1599–1622
- Jiang WS, Luo X, Gao HX, Liang ZW, Liu B, Tontiwachwuthikul P, Hu XY (2018) A comparative kinetics study of CO_2 absorption into aqueous DEEA/MEA and DMEA/MEA blended solutions. *AIChE J* 64(4):1350–1358
- Rashidi NA, Yusup S (2016) An overview of activated carbons utilization for the post-combustion carbon dioxide capture. *J CO₂ Util.* <https://doi.org/10.1016/j.jcou.2015.11.002>
- Jafari T, Moharreri E, Toloueinia P, Amin AS, Sahoo S, Khakpash N, Noshadi I, Alpay SP, Suib SL (2017) Microwave-assisted synthesis of amine functionalized mesoporous polydivinylbenzene for CO_2 adsorption. *J CO₂ Util.* <https://doi.org/10.1016/j.jcou.2017.03.004>
- Papadopoulos AI, Tzirakis F, Tsvintzelis I, Seferlis P (2019) Phase-change solvents and processes for postcombustion CO_2 capture: a detailed review. *Ind Eng Chem Res* 58(13):5088–5111
- Zhao JQ, Lu ZX, He X, Zhang XF, Li QY, Xia T, Zhang W, Lu CH (2017) Fabrication and characterization of highly porous $\text{Fe}(\text{OH})_3$ @cellulose hybrid fibers for effective removal of Congo red from contaminated water. *ACS Sustain Chem Eng* 5(9):7723–7732
- Modak JB, Bhowal A, Datta S (2016) Extraction of dye from aqueous solution in rotating packed bed. *J Hazard Mater* 304:337–342
- Chung KT (2016) Azo dyes and human health: a review. *J Environ Sci Heal C* 34(4):233–261
- Tsai CH, Chang WC, Saikia D, Wu CE, Kao HM (2016) Functionalization of cubic mesoporous silica SBA-16 with carboxylic acid via one-pot synthesis route for effective removal of cationic dyes. *J Hazard Mater* 309:236–248
- Chu FM, Yang LJ, Du XZ, Yang YP (2017) Mass transfer and energy consumption for CO_2 absorption by ammonia solution in bubble column. *Appl Energy* 190:1068–1080
- Han Y, Zhang ZE (2019) Nanostructured membrane materials for CO_2 capture: a critical review. *J Nanosci Nanotechnol* 19(6):3173–3179
- Yang J, Yu XH, An L, Tu ST, Yan JY (2017) CO_2 capture with the absorbent of a mixed ionic liquid and amine solution considering the effects of SO_2 and O_2 . *Appl Energy* 194:9–18
- Singh G, Lakhi KS, Sil S, Bhosale SV, Kim I, Albahily K, Vinu A (2019) Biomass derived porous carbon for CO_2 capture. *Carbon* 148:164–186
- Banaszkiewicz T, Chorowski M (2018) Energy consumption of air-separation adsorption methods. *Entropy* 20(4):232
- Ma R, Hao J, Chang GZ, Wang YX, Guo QJ (2020) Nitrogen-doping microporous adsorbents prepared from palm kernel with excellent CO_2 capture property. *C J Chem Eng* 98(2):503–512
- Li Y (2021) Research progress of hydrogen sulfide adsorption based on MOFs. *ChemistrySelect* 6(37):9960–9968
- Zhang S, Li M, Li W, Li YW, Liu F, Xue M, Wang YQ, Zhang CC (2021) Comparison and analysis of toluene adsorption properties of ZSM-5 molecular sieve treated by different modification methods: adsorption kinetic and mechanism studies. *Chin Pet Process Pe Technol* 23(1):76–87
- Szczesniak B, Choma J (2020) Graphene-containing microporous composites for selective CO_2 adsorption. *Micropor Mesopor Mat* 292:109761
- Guo YF, Tan C, Sun J, Li WL, Zhang JB, Zhao CW (2020) Porous activated carbons derived from waste sugarcane bagasse for CO_2 adsorption. *Chem Eng J* 381:122736
- Rao TM, Rao WB (2016) Biosorption of Congo red from aqueous solution by crab shell residue: a comprehensive study. *Springerplus* 5:537
- Sevilla M, Fuertes AB (2014) Direct synthesis of highly porous interconnected carbon nanosheets and their application as high-performance supercapacitors. *ACS Nano* 8(5):5069–5078
- Li JX, Chen XC, Gong J, Zhu JY, Mijowska E (2020) Deep insight into the pore size distribution of N-doped porous carbon materials on electrochemical energy storage and CO_2 sorption. *Diam Relat Mater* 105:107802
- Chen HX, Xia W, Wang N, Liu Y, Fan PH, Wang S, Li SX, Liu J, Tang T, Zhang AL, Ding Z, Wu WD, Chen Q (2022) Flame retardancy of biodegradable polylactic acid with piperazine pyrophosphate and melamine cyanurate as flame retardant. *J Fire Sci* 40(4):254–273

30. Wang S, Wu WD, Chen Q, Ding Z, Li SX, Zhang AL, Tang T, Liu J, Okoye PU (2022) Preparation of DOPO-derived magnesium phosphate whisker and its synergistic effect with ammonium polyphosphate on the flame retardancy and mechanical property of epoxy resin. *J Appl Polym Sci*. e53430 <https://doi.org/10.1002/app.53430>
31. Chen HX, Xia W, Wang S (2022) Biodiesel production from waste cooking oil using a waste diaper derived heterogeneous magnetic catalyst. *Braz J Chem Eng*. <https://doi.org/10.1007/s43153-022-00257-z>
32. El Khomri M, El Messaoudi N, Dbik A, Bentahar S, Fernine Y, Lacherai A, Jada A (2022) Optimization based on response surface methodology of anionic dye desorption from two agricultural solid wastes. *Chem Afr* 5:1083–1095
33. Yue LM, Xia QZ, Wang LW, Wang LL, DaCosta H, Yang J, Hu X (2018) CO₂ adsorption at nitrogen-doped carbons prepared by K₂CO₃ activation of urea-modified coconut shell. *J Colloid Interf Sci* 511:259–267
34. El Khomri M, El Messaoudi N, Dbik A, Bentahar S, Lacherai A, Chegini ZG, Bouich A (2022) Removal of Congo red from aqueous solution in single and binary mixture systems using Argan nutshell wood. *Pigm Resin Technol* 51(5):477–488
35. El Khomri M, El Messaoudi N, Dbik A, Bentahar S, Lacherai A, Chegini ZG, Iqbal M (2022) Organic dyes adsorption on the almond shell (*Prunus dulcis*) as agricultural solid waste from aqueous solution in single and binary mixture systems. *Bioinert Res Appl Chem* 12(2):2022–2040
36. Pereira PHF, Oliveira TIS, Rosa MF, Cavalcante FL, Moates GK, Wellner N, Waldron KW, Azeredo HMC (2016) Pectin extraction from pomegranate peels with citric acid. *Int J Biol Macromol* 88:373–379
37. Luo XD, Li SY, Xu HY, Zou XH, Wang Y, Cheng J, Li X, Shen ZF, Wang YG, Cui LF (2021) Hierarchically porous carbon derived from potassium-citrate-loaded poplar catkin for high performance supercapacitors. *J Col Interf Sci* 582:940–949
38. Rathinam K, Singh SP, Arnusch CJ, Kasher R (2018) An environmentally-friendly chitosan-lysozyme biocomposite for the effective removal of dyes and heavy metals from aqueous solutions. *Carbohydr Polym* 199:506–515
39. Geng JJ, Yin YM, Liang QW, Zhu ZJ, Luo HJ (2019) Polyethyleneimine cross-linked graphene oxide for removing hazardous hexavalent chromium: adsorption performance and mechanism. *Chem Eng J* 361:1497–1510
40. Ali H, Ismail AM (2022) Fabrication of magnetic Fe₃O₄/Polypyrrole/carbon black nanocomposite for effective uptake of Congo red and methylene blue dye: adsorption investigation and mechanism. *J Polym Environ*. <https://doi.org/10.1007/s10924-022-02663-3>
41. Chen C, Yu DF, Zhao GY, Du BS, Tang W, Sun L, Sun Y, Besenbacher F, Yu M (2016) Three-dimensional scaffolding framework of porous carbon nanosheets derived from plant wastes for high-performance supercapacitors. *Nano Energy* 27:377–389
42. Ma CD, Gong J, Zhao S, Liu XG, Mu XY, Wang YH, Chen XC, Tang T (2022) One-pot green mass production of hierarchically porous carbon via a recyclable salt-templating strategy. *Green Energy Environ* 7(4):818–828
43. Uner O, Gecgel U, Avcu T (2021) Comparisons of activated carbons produced from sycamore balls, ripe black locust seed pods, and nerium oleander fruits and also their H₂ storage studies. *Carbon Lett* 31(1):75–92
44. Saleh M, Tiwari JN, Kemp KC, Yousuf M, Kim KS (2013) Highly selective and stable carbon dioxide uptake in polyindole-derived microporous carbon materials. *Environ Sci Technol* 47(10):5467–5473
45. Wei HM, Chen HJ, Fu N, Chen J, Lan GX, Qian W, Liu YP, Lin HL, Han S (2017) Excellent electrochemical properties and large CO₂ capture of nitrogen-doped activated porous carbon synthesised from waste longan shells. *Electrochim Acta* 231:403–411
46. Qiu ZP, Wang YS, Bi X, Zhou T, Zhou J, Zhao JP, Miao ZC, Yi WM, Fu P, Zhuo SP (2018) Biochar-based carbons with hierarchical micro-meso-macro porosity for high rate and long cycle life supercapacitors. *J Power Sources* 376:82–90
47. Coromina HM, Walsh DA, Mokaya R (2016) Biomass-derived activated carbon with simultaneously enhanced CO₂ uptake for both pre and post combustion capture applications. *J Mater Chem A* 4(1):280–289
48. Lei L, Cheng Y, Chen CW, Kosari M, Jiang ZY, He C (2022) Taming structure and modulating carbon dioxide (CO₂) adsorption isosteric heat of nickel-based metal organic framework (MOF-74(Ni)) for remarkable CO₂ capture. *J Col Interf Sci* 612:132–145
49. Nazir G, Rehman A, Park SJ (2022) Self-activated, urea modified microporous carbon cryogels for high-performance CO₂ capture and separation. *Carbon* 192:14–29
50. Hou LQ, Yang W, Jiang B, Wang P, Yan L, Zhang CX, Huang GY, Yang F, Li YF (2021) Intrinsic defect-rich porous carbon nanosheets synthesized from potassium citrate toward advanced supercapacitors and microwave absorption. *Carbon* 183:176–186
51. Tiwari D, Bhunia H, Bajpai PK (2018) Development of chemically activated N-enriched carbon adsorbents from urea-formaldehyde resin for CO₂ adsorption: kinetics, isotherm, and thermodynamics. *J Environ Manag* 218:579–592
52. Li JX, Michalkiewicz B, Min JK, Ma CD, Chen XC, Gong J, Mijowska E, Tang T (2019) Selective preparation of biomass-derived porous carbon with controllable pore sizes toward highly efficient CO₂ capture. *Chem Eng J* 360:250–259
53. Tiwari D, Bhunia H, Bajpai PK (2018) Adsorption of CO₂ on KOH activated, N-enriched carbon derived from urea formaldehyde resin: kinetics, isotherm and thermodynamic studies. *Appl Surf Sci* 439:760–771
54. Goel C, Bhunia H, Bajpai PK (2015) Resorcinol-formaldehyde based nano-structured carbons for CO₂ adsorption: kinetics, isotherm and thermodynamic studies. *RSC Adv* 5(113):93563–93578
55. Goel C, Bhunia H, Bajpai PK (2015) Synthesis of nitrogen doped mesoporous carbons for carbon dioxide capture. *RSC Adv* 5(58):46568–46582
56. Choi SW, Tang JL, Pol VG, Lee KB (2019) Pollen-derived porous carbon by KOH activation: effect of physicochemical structure on CO₂ adsorption. *J CO₂ Util* 29:146–155
57. Rao LL, Liu SF, Wang LL, Ma CD, Wu JY, An LY, Hu X (2019) N-doped porous carbons from low-temperature and single-step sodium amide activation of carbonized water chestnut shell with excellent CO₂ capture performance. *Chem Eng J* 359:428–435
58. Palacios T, Hsu A, Wang H (2010) Applications of graphene devices in RF communications. *Ieee Communi Mag* 48(6):122–128
59. Ismail IS, Singh G, Smith P, Kim S, Yang J-H, Joseph S, Yusup S, Singh M, Bansal V, Talapaneni SN, Vinu A (2020) Oxygen functionalized porous activated biocarbons with high surface area derived from grape marc for enhanced capture of CO₂ at elevated-pressure. *Carbon* 160:113–124
60. Igalavithana AD, Choi SW, Dissanayake PD, Shang J, Wang CH, Yang X, Kim S, Tsang DCW, Lee KB, Ok YS (2020) Gasification biochar from biowaste (food waste and wood waste) for effective CO₂ adsorption. *J Hazard Mater* 391:121147
61. Shi JS, Yan NF, Cui HM, Xu JG, Liu YW, Zhang SW (2019) Salt template synthesis of nitrogen and sulfur co-doped porous carbons as CO₂ adsorbents. *ACS Sustain Chem Eng* 7(24):19513–19521
62. Kalyani G, Gokulan R, Sujatha S (2021) Biosorption of zinc metal ion in aqueous solution using biowaste of pithophora cleveana wittrock and mimusops elengi. *Desalin Water Treat* 218:363–371
63. El Khomri M, El Messaoudi N, Dbik A, Bentahar S, Lacherai A (2020) Efficient adsorbent derived from argania spinosa for the adsorption of cationic dye: kinetics, mechanism, isotherm and thermodynamic study. *Surf Interfaces* 20:10060
64. Mohammed AA, Kareem SL (2021) Enhancement of ciprofloxacin antibiotic removal from aqueous solution using ZnO nanoparticles coated on pistachio shell. *Desalin Water Treat* 213:229–239
65. Miandad R, Kumar R, Barakat MA, Basheer C, Aburiazza AS, Nizami AS, Rehan M (2018) Untapped conversion of plastic waste char into carbon-metal LDOs for the adsorption of Congo red. *J Col Interf Sci* 511:402–410
66. Huang ZY, Wu P, Yin YK, Zhou X, Fu L, Wang LX, Chen SH, Tang X (2022) Preparation of pyridine-modified cotton fibers for anionic dye treatment. *React Funct Polym* 172:105155
67. Zair ZR, Alismaeel ZT, Eyssa MY, M-Ridha MJ (2022) Optimization, equilibrium, kinetics and thermodynamic study of congo red dye adsorption from aqueous solutions using iraqi porcelanite rocks. *Heat Mass Transfer* 58(8):1393–1410
68. Stawinski W, Wegrzyn A, Freitas O, Chmielarz L, Mordarski G, Figueiredo S (2017) Simultaneous removal of dyes and metal cations using an acid, acid-base and base modified vermiculite as a sustainable and recyclable adsorbent. *Sci Total Environ* 576:398–408
69. Yu JD, Jiang CY, Guan QQ, Ning P, Gu JJ, Chen QL, Zhang JM, Miao RR (2018) Enhanced removal of Cr(VI) from aqueous solution by supported

ZnO nanoparticles on biochar derived from waste water hyacinth. *Chemosphere* 195:632–640

70. Quan XP, Sun ZQ, Meng H, Han YD, Wu JB, Xu JL, Xu Y, Zhang X (2019) Polyethyleneimine (PEI) incorporated Cu-BTC composites: extended applications in ultra-high efficient removal of congo red. *J Solid State Chem* 270:231–241
71. Shabani S, Dinari M (2022) Itaconic acid-modified layered double hydroxide/gellan gum nanocomposites for Congo red adsorption. *SCI REP-UK* 12(1):4356
72. Zubir MHM, Zaini MAA (2020) Twigs-derived activated carbons via $H_3PO_4/ZnCl_2$ composite activation for methylene blue and congo red dyes removal. *SCI REP-UK* 10:14050
73. Ojedokun AT, Bello OS (2017) Kinetic modeling of liquid-phase adsorption of Congo red dye using guava leaf-based activated carbon. *Appl Water Sci* 7:1965–1977

Publisher's Note

Springer Nature remains neutral with regard to jurisdictional claims in published maps and institutional affiliations.

Submit your manuscript to a SpringerOpen[®] journal and benefit from:

- ▶ Convenient online submission
- ▶ Rigorous peer review
- ▶ Open access: articles freely available online
- ▶ High visibility within the field
- ▶ Retaining the copyright to your article

Submit your next manuscript at ▶ [springeropen.com](https://www.springeropen.com)
